

Feasibility Studies of a Nuclei Trigger using the ALICE-TRD

BACHELORARBEIT
am Institut für Kernphysik Frankfurt

vorgelegt von
BENJAMIN BRUDNYJ

Fachbereich Physik
der Goethe-Universität
Frankfurt am Main

Juni 2019

Erstgutachter: Prof. Dr. C. Blume
Zweitgutachter: Dr. B. Döningus

Abstract

At the Large Hadron Collider (LHC) at CERN significant production rates of light (anti-) (hyper-)nuclei have been measured in Pb–Pb collisions. The investigation of such nuclei has recently become a topic of high interest. For instance the measured lifetime of the lightest hypernucleus, the hypertriton (a bound state of a proton, a neutron and a Λ hyperon), is significantly below the expectation of state-of-the-art theory calculations, which expect the lifetime to be very close to the Λ lifetime. Therefore, it is important to also measure these rarely produced hyper-nuclei in pp collisions to check, whether the shorter lifetime is an effect of heavy-ion collisions.

Due to its short lifetime and decay length ($c\tau \approx 7$ cm for ${}^3_{\Lambda}\text{H}$) only its decay products can be measured in TPC, TRD and TOF detectors, e.g. the decay products of the charged two-body decay channel ${}^3_{\Lambda}\text{H} \rightarrow {}^3\text{He} + \pi^-$. In order to be able to measure these rare decays also in pp and p–Pb collisions, it is essential to increase the statistics by employing a trigger on nuclei. Using the data on Pb–Pb collisions at $\sqrt{s_{\text{NN}}} = 2.76$ TeV it could be shown out that particles with $Z > 1$ in the TRD have properties that can be used to implement such a nuclei trigger.

In this thesis the physics case of a nuclei trigger will be elaborated as well as the extracted trigger efficiencies and purities for the different light nuclei, i.e. (anti-)d, (anti-)t, (anti-) ${}^3\text{He}$ and (anti-) ${}^4\text{He}$.

Kurzfassung

Am Large Hadron Collider (LHC) am CERN sind in Pb–Pb Kollisionen signifikante Produktionsraten von leichten (Anti-)Hyper-Kernen gemessen worden. Die Produktion solcher Kerne ist in jüngster Zeit zu einem Thema von großem Interesse geworden. Zum Beispiel ist die gemessene Lebensdauer des leichtesten Hyperkerns, dem Hypertriton (ein schwach gebundener Zustand eines Protons, eines Neutrons und eines Lambda-Hyperons Λ), erheblich kleiner als die Erwartung aus den aktuellen theoretischen Berechnungen, welche eine Lebensdauer nahe der des Λ vorhersagt. Deshalb ist es wichtig diese selten produzierten Kerne auch in pp Kollisionen zu messen, um zu überprüfen, ob die kleinere Lebensdauer ein Effekt der Schwerionen-Kollisionen ist.

Aufgrund der geringen Lebensdauer und kleinen Zerfallslängen ($c\tau \approx 7$ cm des $^3\Lambda$ H) dieser seltenen Teilchen, können in den Detektoren TPC, TRD und TOF nur ihre Zerfallsprodukte detektiert werden, z.B. der geladene Zwei-Körper-Zerfallskanal $^3\Lambda$ H \rightarrow 3 He + π^- . Um diese Zerfälle ebenfalls in pp und in p–Pb Kollisionen messen zu können, ist es unerlässlich die Statistik durch einen Trigger auf leichte (Anti-)Kerne zu verbessern. Mit Hilfe eines Datensatzes von Pb–Pb Kollisionen bei der Energie von $\sqrt{s_{NN}} = 2.76$ TeV konnte gezeigt werden, dass Teilchen mit $Z > 1$ im Übergangsstrahlungsdetektor (TRD) bestimmte Eigenschaften haben, die benutzt werden können, um den erforderlichen Trigger zu realisieren.

In dieser Bachelorarbeit wird die Machbarkeit eines Triggers auf leichte Kerne ausgearbeitet, sowie die Trigger Effizienzen und Reinheiten für verschiedene leichte Kerne, z.B. (Anti-)d, (Anti-)t, (Anti-) 3 He and (Anti-) 4 He.

Contents

1	Introduction and Motivation	1
2	A Large Ion Collider Experiment (ALICE)	4
2.1	ALICE at the LHC	4
2.1.1	TPC	5
2.1.2	TRD	6
2.1.3	TOF	6
2.2	The Transition Radiation Detector (TRD)	7
2.3	Electronics overview and Trigger system	8
3	Theoretical and Technical Backround	10
3.1	Dataset	10
3.2	Specific energy loss	10
3.3	Transverse momentum p_T	13
3.4	Charge deposition in the TRD	15
4	Feasibility Study on Real Data	19
4.1	Trigger concept	19
4.1.1	Purity, trigger efficiency, rejection factor	21
4.2	Results	21
4.2.1	Purity	22
4.2.2	Trigger efficiency	23
4.2.3	Rejection factor	24
4.3	p_T dependence	25
4.4	Conclusion	26
5	Trigger Tests	27
5.1	Look-up table	27
5.2	Settings for TRD triggers	28
5.3	First look into new data	28
6	Summary and Outlook	30
	Bibliography	33

1 Introduction and Motivation

In the standard model of particle physics the known elementary particles and fundamental forces in the universe are described. There are six different quarks (up, down, charm, strange, top, bottom), which form the hadrons. Baryons and mesons are hadrons consisting of three, respectively two quarks. The dominating two baryons in nature are protons (consisting of two up-quarks and one down-quark) and neutrons (consisting of one up-quark and two down-quarks) which are the only two constituents of the table of nuclides, which is often called Segrè chart. In figure 1.1 one can see a part of this table of nuclides with an added third axis, the strangeness S . Nuclei with e.g. a Λ -baryon (consisting of one up-quark, one down quark and one strange-quark) instead of neutrons are the so-called hypernuclei, where the hypertriton ${}^3_{\Lambda}\text{H}$ is the lightest one.

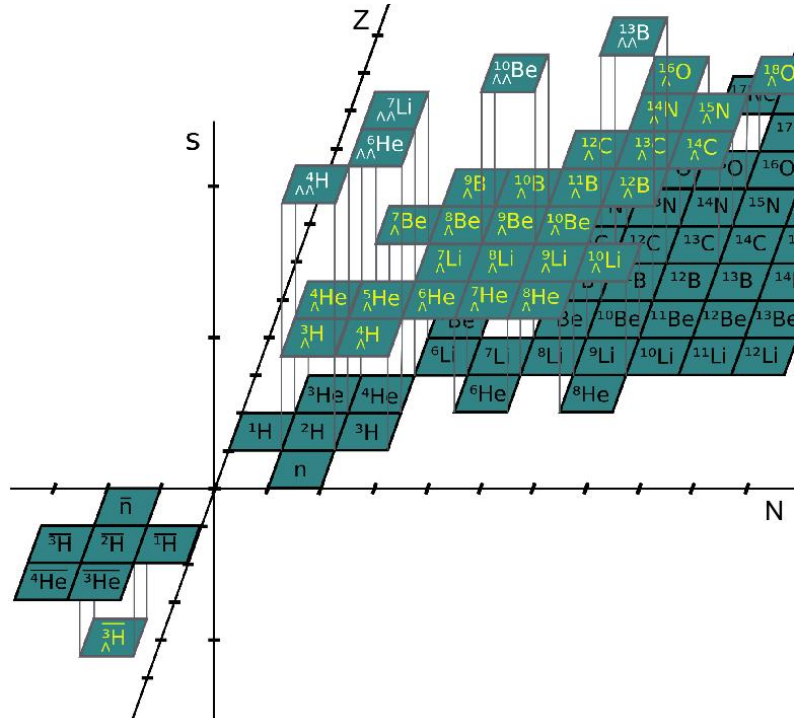
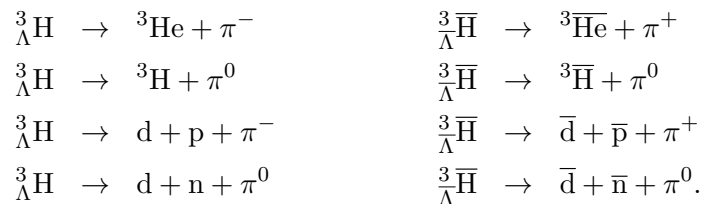


Figure 1.1: Extended table of nuclides with Z the number of protons, N the number of neutrons and an added axis of strangeness S [GSI 15].

With experiments in high-energy physics it is possible to study particles and light nuclei and e.g. their production mechanism and lifetimes. However, the production rates of light nuclei are very small in comparison to particles like pions, protons, electrons, kaons and other commonly produced particles. An issue of small production rates is, that it is difficult to collect sufficient statistics for a significant measurement, so the results of different experiments are very fluctuating. The mentioned hypertriton is a bound system of a proton, a neutron and a Λ -baryon with the following π -mesonic decay modes [KAM 98]:



The production yields of ${}^3_{\Lambda}\text{H}$ and its anti-nucleus ${}^3_{\bar{\Lambda}}\text{H}$ are measured by detecting their mesonic decay via the topological identification of secondary vertices and the analysis of the invariant mass distribution [ALI 16]. The $dN/d(ct)$ distribution were used to determine the lifetime τ . Theoretical calculations of the mesonic and non-mesonic decay of the hypertriton predict total lifetime of ${}^3_{\Lambda}\text{H}$ to be 256 ps [KAM 98], which is close to the lifetime of a free Λ of 263.2 ± 2.0 ps [PDG 14]. In the past decades the hypertriton lifetime was measured by different collaborations, which is shown in figure 1.2. Here, the combined average value of the lifetime is presented, which is about 30% smaller than τ_Λ [GAL 18], see dashed line. This issue represents the so-called "hypertriton lifetime puzzle".

The latest ALICE result, which is shown in figure 1.2, on hypertriton lifetime and decay length, measured in Pb–Pb collisions at $\sqrt{s_{\text{NN}}} = 5.02$ TeV, is the following [TRO 18]:

$$\begin{aligned} \tau &= 237^{+33}_{-36}(\text{stat.}) \pm 17(\text{syst.})\text{ps} \\ c\tau &= 7.10^{+1.00}_{-1.07}(\text{stat.}) \pm 0.50(\text{syst.})\text{cm}. \end{aligned}$$

In figure 1.2 one also can see the big uncertainties of the early results. This is due to the small yields and therefore low statistics on this rare hypernucleus. A solution of this issue is to increase the dataset, but for this approach the accelerator properties and the storage space are not sufficient. A more promising solution is to implement a trigger, so only events with a high probability to find light nuclei will be stored.

As such, one goal is to obtain more precise results. However, one can also assume that the lower lifetime in recent measurements is a result of effects present only in heavy-ion collisions. To investigate this assumption it is essential to compare the results with those, which are produced in proton–proton collisions. But up to now no ${}^3_{\Lambda}\text{H}$ is observed in pp

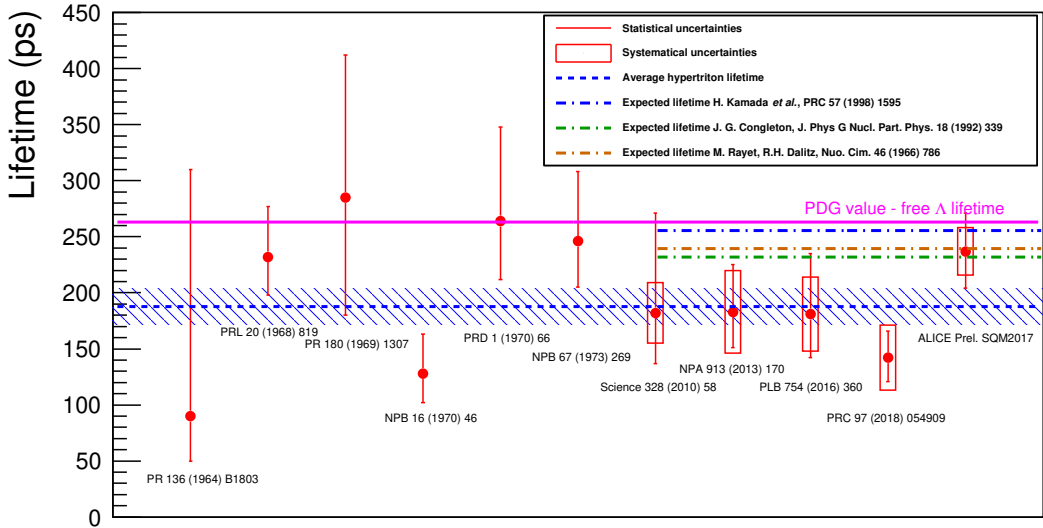


Figure 1.2: Hypertriton lifetime measured by different collaborations [GAL 18].

collisions. Therefore, a further goal is to measure hypertritons and other not seen light nuclei in these elementary collisions for the first time. Figure 1.1 shows only all confirmed nuclei, hypernuclei and their corresponding anti-nucleus which are measured up to date.

Especially the anti-alpha ${}^4\bar{\text{He}}$ is a nucleus of high interest, because it is not observed neither in pp nor in p–Pb collisions.

These rare probes need to be enhanced with a trigger. Therefore, such a nuclei trigger is required to increase the statistics, which is a fundamental step forwards solving those interesting questions and problems in particle physics.

2 A Large Ion Collider Experiment (ALICE)

The ALICE detector is one of the four big experiments at the worlds largest collider, the Large Hadron Collider (LHC) at the European Organization for Nuclear Research (CERN) in France and Switzerland. The LHC can provide several collision systems at various energies and ALICE is the only dedicated heavy-ion experiment at this accelerator.

2.1 ALICE at the LHC

With the high temperatures and energy densities created in heavy-ion collisions a phase transition of matter from a state of hadronic constituents into a plasma of deconfined quarks and gluons – the quark-gluon plasma (QGP) – is predicted [PBM 03]. With these experiments it is possible to produce and study the QGP. The crossing point of the beam-lines of the LHC, which is also the collision point, is in the area of the center of the Inner Tracking System (ITS), as shown in figure 2.1. The ITS is a system of Silicon Pixel Detectors (SPD) for the innermost two layers, Silicon Drift Detectors (SDD) for the following two layers and double-sided Silicon Strip Detectors (SSD) for the two outer layers.

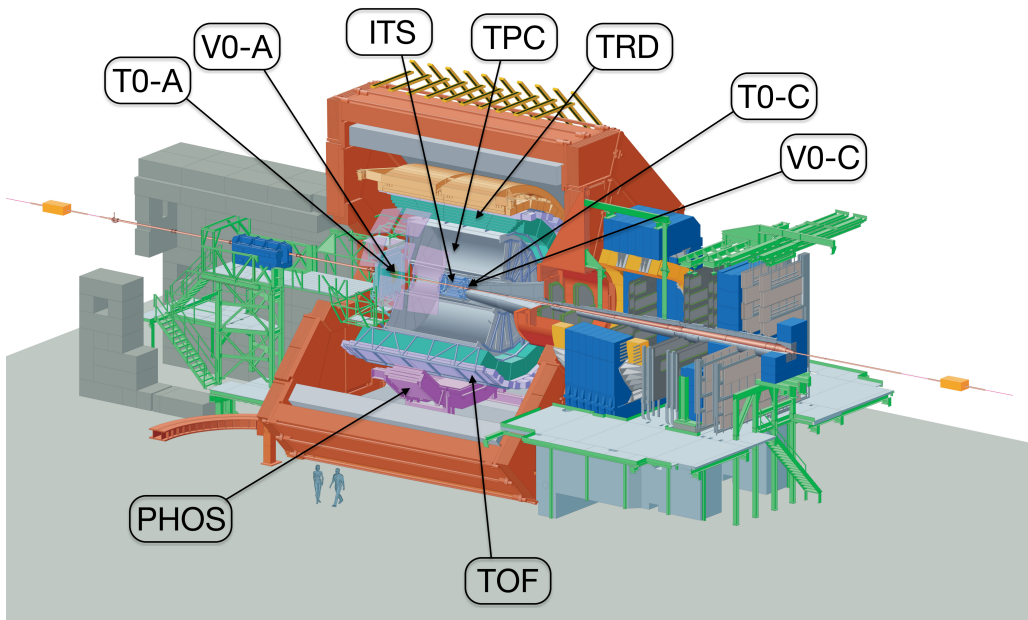


Figure 2.1: Sketch of the ALICE experiment.

The main tasks of the ITS are among others to localize the primary vertex and to reconstruct the secondary vertices from decays of e.g. a hypertriton [ALI 08]. At small radial distances from the beam line there are also installed the forward detectors V0 and T0 to provide the level-0 trigger and multiplicity information in forward and backward regions. V0 consists of two areas of cherenkov radiators, one at the A-side and one at the C-side. T0 consists of two rings of plastic scintillators, also one on each side [ALI 04]. To describe the acceptance of the TRD detector (see section 2.1.2) one has to consider the "PHOS-hole", an area of three TRD supermodules, where several chambers are not installed to ensure a better performance of the PHOS detector, which is an electromagnetic calorimeter, devoted to the study of electromagnetic signals [ALI 99]. To identify all produced particles ALICE is using a set of 18 different detectors to measure all relevant information of the particles. In the following the detectors contributing to this feasibility study will be introduced.

2.1.1 TPC

The Time Projection Chamber (TPC) is a gas filled detector of cylindrical shape with a full azimuthal coverage. It is the main device for tracking and identification of charged particles in the central barrel.

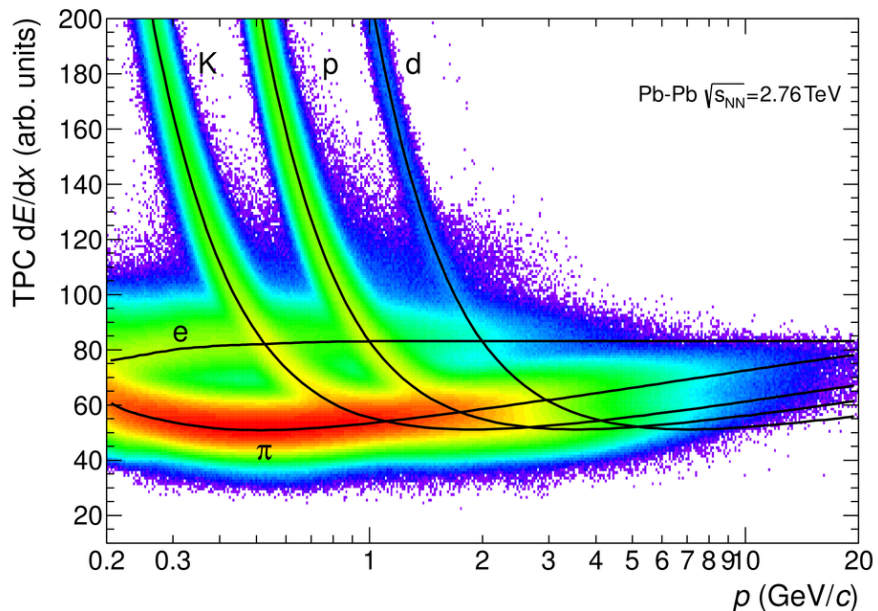


Figure 2.2: Specific energy loss (dE/dx) in the TPC as a function of particle momentum in Pb–Pb collisions at $\sqrt{s_{NN}} = 2.76$ TeV . The lines represent the Bethe-Bloch parameterization of the expected mean energy loss of different particle species [ALI 14].

Its volume is about 90 m^3 and covers the pseudorapidity range $|\eta| < 0.9$, which matches the acceptance of the ITS, TRD and TOF detectors [ALI 00]. Traversing charged particles ionize the gas molecules and thus produce primary electrons. An electric field transports these electrons to the Multi Wire Proportional Chambers (MWPC) to the endplate of the TPC. After a first signal amplification they influence a signal on the pad plane, where it gets amplified and digitized by front-end electronics. The detector provides an excellent momentum and energy-loss resolution, however with a drift time of $\approx 88 \mu\text{s}$ [ALI 10].

2.1.2 TRD

After traversing ITS and TPC the particles reach the Transition Radiation Detector (TRD). Due to the importance of the detector in this thesis a more detailed description will be provided in section 2.2.

2.1.3 TOF

The Time-Of-Flight (TOF) detector consists of Multigap Resistive Plate Chambers (MRPC) and was proposed with the purpose for identifying charged particles in the intermediate momentum range [ALI 02]. It is the outermost detector in the central barrel.

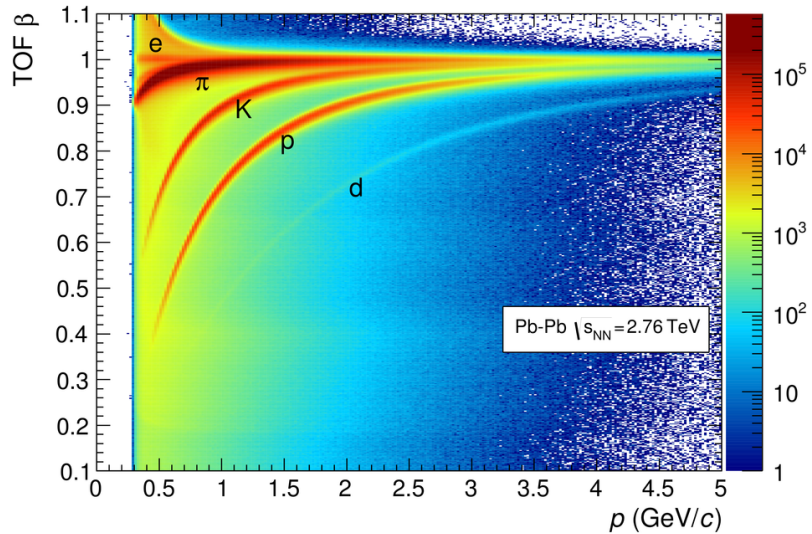


Figure 2.3: Distribution of β , the relation between the particle velocity to the speed of light, as a function of momentum p measured by the TOF in Pb–Pb collisions at $\sqrt{s_{\text{NN}}} = 2.76 \text{ TeV}$ [ALI 14].

This detector measures the time of arrival for particles coming from the collision point. As a starting point the detectors T0-A and T0-C are used with a time resolution of 20-25 ps in Pb–Pb collisions and ≈ 40 ps in pp collisions [ALI 14]. With the time of flight information it is possible to obtain the velocity and thereby the mass of the particles. In low and intermediate momentum range the measured particles are well distinguishable as seen in figure 2.3.

2.2 The Transition Radiation Detector (TRD)

The TRD was designed and built to discriminate between electrons and pions in the region where the TPC is no longer sufficient. With its help ALICE is able to identify electrons and trigger on them. The TRD and the other detectors in the central barrel are located inside a solenoid magnet, which provides a magnetic field of $B = 0.5$ T. The detector consists of 18 supermodules, as can be seen in figure 2.6. Every supermodule is segmented in 5 stacks, each with 6 tracking chambers (see figure 2.5). In total, the number of installed read-out chambers is only 521, because in sector 13-15 there are chambers not installed to ensure a better performance of the PHOS detector. Every read-out chamber is filled with a Xe-CO₂ (85/15) gas mixture. The radiator material is a fibre/foam sandwich [ALI 17]. A characteristic property of the different materials is the refraction index $n = \sqrt{\epsilon\mu}$, where ϵ is the relative permittivity and μ is the relative permeability. The transition of highly relativistic particles between two different materials causes the emission of transition radiation, which depends on the Lorentz-factor $\gamma = \frac{1}{\sqrt{1-\beta^2}} = \frac{E}{m}$, where $c = 1$. Therefore, the light electron causes a measurable emission photon, as illustrated in figure 2.4. In addition to the characteristic transition radiation, the traversing particles interact with the gas and ionize its atoms, as described in section 3.4.

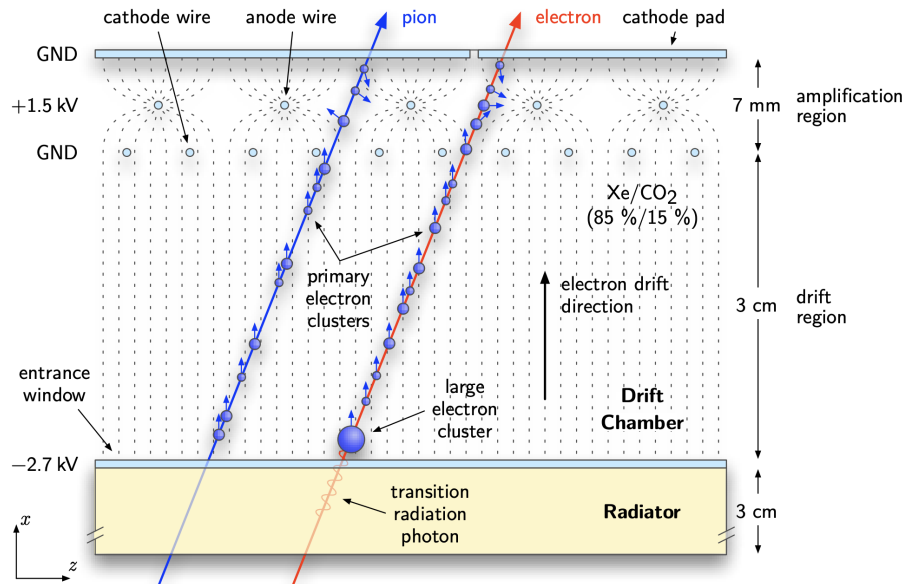


Figure 2.4: Cross section of a TRD chamber. A traversing charged particle deposits energy in the drift region via ionisation, while the light electron causes in addition the emission of transition radiation [CUV 09].

Charged particles passing through the drift chamber deposit energy by ionization. The resulting amount of electrons is proportional to the particle velocity. The electrons will drift to the anode, where the signal is amplified. After a first amplification the electrons

influence charge on the read-out pads, that will be further described in the next section. The TRD provides the possibility to decide via a level-1 trigger, only 6.5 μ s after a level-0 trigger, whether an event is an interesting one (see section 2.3) [KLE 11]. So, only when at least 4 tracklets of one stack fulfill a fixed trigger condition, the event is stored.

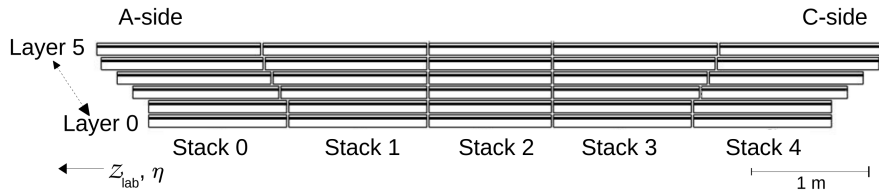


Figure 2.5: Cross section of a TRD supermodule. One can see the segmentation in 5 stacks each with 6 tracking chambers [ALI 17].

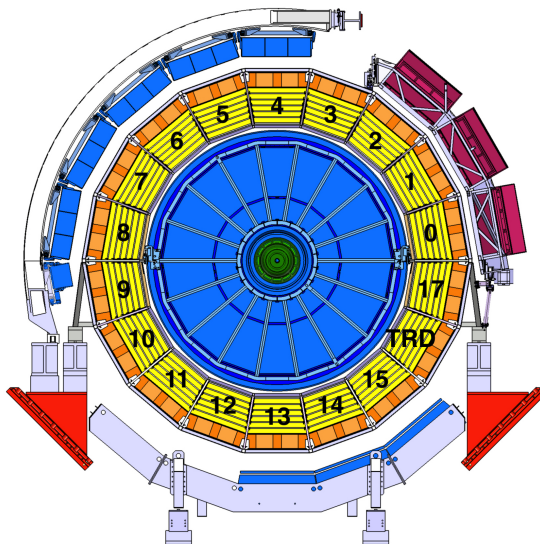


Figure 2.6: Cross section of the ALICE detector perpendicular to the LHC beam direction. The 18 supermodules of the TRD are shown in yellow. In sector 13-15 there is the "PHOS-hole", where several TRD chambers are not installed.

2.3 Electronics overview and Trigger system

Figure 2.7 illustrates the Front-End Electronics (FEE) with its main component the Multi-Chip Module (MCM) located directly on the chamber. It consists of a PASA (PreAmplifier and ShAper) and a TRAP (TRAcklet Processor) chip. The first part in the TRAP chip is a Analog-to-Digital Converter (ADC), where the measured deposited charges are converted into bit values. To reduce the power consumption the detector remains in a sleep mode during inactive phases. Therefore, the TRD FEE requires a fast wake-up signal. For Run-1 a pretrigger is used as a wake-up signal, either from the forward detectors V0 or T0 or the TOF detector to start data processing and acquisition. For Run-2 the functionality of

that pretrigger could be integrated in the Central Tracking Unit (CTP) and is now called LM (level minus 1) trigger. An interface unit (LTU-T) was then developed to provide the requirements of the FEE [ALI 17]. After that a level-0 trigger can decide to abort the processing 1.2 μ s after the collision.

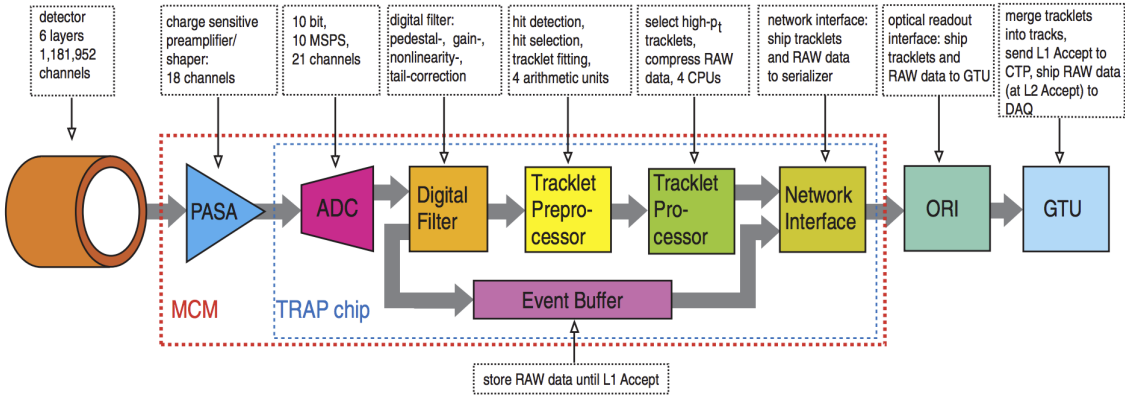


Figure 2.7: TRD readout electronics. The Multi-Chip Module (MCM) and the Optical Readout Interface (ORI) are directly mounted on the detector modules [ALI 08].

The processing continues if a level-0 trigger is received. If a signal fulfills the trigger condition the tracklet processor merge the signals of primary electron clusters of a chamber into tracklets and the Optical Readout Interface (ORI) ships the data to the Global Tracking Unit (GTU) outside the L3 magnet, where the tracklets are merged into tracks [ALI 17]. These tracks are used for the level-1 trigger conditions. As just discussed, the level-1 trigger can accept the tracks after further 6.5 μ s. The GTU then ships the accepted level-1 tracks to the level-2 trigger, which depends on the drifttime in the TPC. Therefore, it needs about 100 μ s after the collision to receive a level-2 decision [KLE 11]. After a level-2 accept the Data AcQuisition System (DAQ) stores the received data.

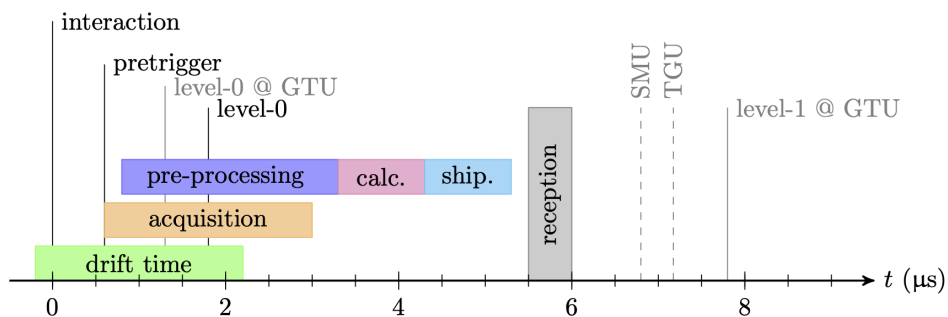


Figure 2.8: Trigger timing relative to the interaction [ALI 17].

3 Theoretical and Technical Background

In this chapter the dataset used for the feasibility study and the physical explanations of the used parameters will be presented.

3.1 Dataset

The study in chapter 4 is based on real data on Pb–Pb collisions at $\sqrt{s_{NN}} = 2.76$ TeV measured by ALICE in 2011. The investigated dataset is part of LHC11h pass2. This part has a total number of 6.2×10^6 events [ALI WIK] with about 252.1×10^6 identified tracks. In this dataset only the tracks were stored, which were measured both in the TPC and the TRD, i.e. all tracks, which are not matching, were rejected. So, the total number of stored tracks are equal in those detectors.

3.2 Specific energy loss

When fast charged particles traverse matter, e.g. the TPC gas, they interact with electrons of the gas atoms. This causes a specific energy loss dE per traveled distance dx , which is described by Hans Bethe in 1932 [BET 32] and Felix Bloch in 1933 [BLO 33] with the relativistic Bethe-Bloch formula [LOE 18]

$$-\frac{dE}{dx} = K z^2 \frac{Z}{A} \frac{1}{\beta^2} \left[\frac{1}{2} \ln \left(\frac{2m_e c^2 \beta^2 \gamma^2 T_{max}}{I^2} \right) - \beta^2 - \frac{\delta(\beta\gamma)}{2} \right], \quad (3.1)$$

with the following parameters:

- $\beta = \frac{v}{c}$
- $\gamma = \frac{1}{\sqrt{1-\beta^2}}$
- particle velocity v
- speed of light c
- charge number of the projectile particle z
- elementary charge e
- rest mass of the electron m_e

- atomic number of absorber Z
- atomic mass of absorber A
- mean excitation energy I
- maximum kinetic energy T_{max} which can be transferred to a free electron in a single collision
- constant $K = 4\pi N_A r_e^2 m_e c^2$
- Avogadro's number N_A
- classical electron radius r_e
- density effect correction to ionization energy loss $\delta(\beta\gamma)$

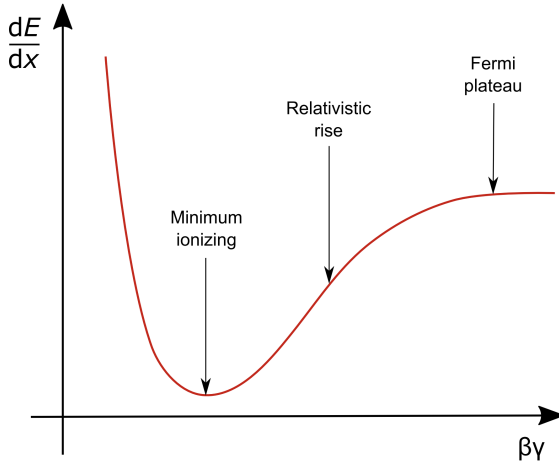
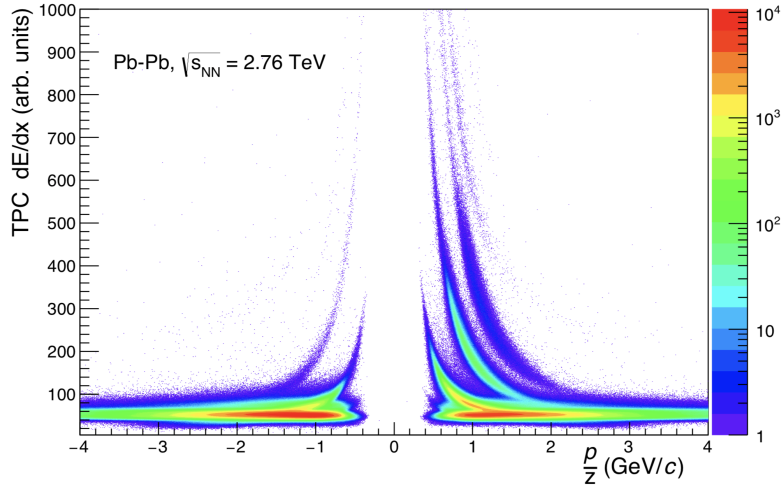


Figure 3.1: Specific energy loss as a function of $\beta\gamma$ [LOE 18].

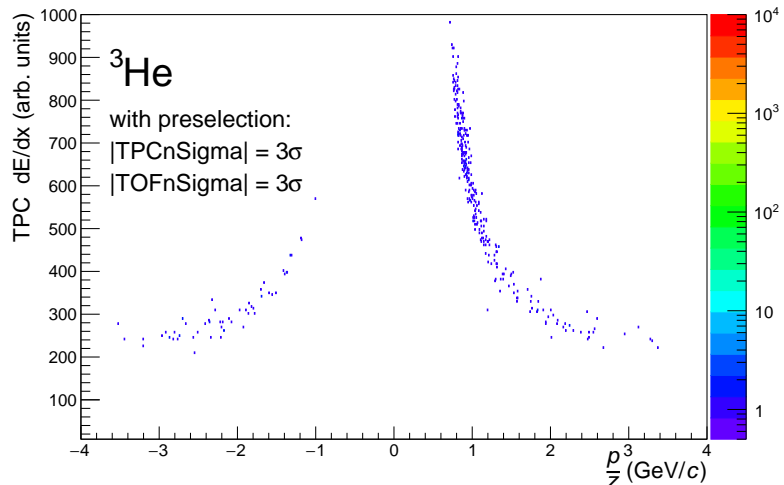
In figure 3.1 the specific energy loss as a function of $\beta\gamma$ is shown. Here $\beta\gamma = \frac{p}{Mc}$ of the crossing particle. The energy loss becomes smaller for increasing $\beta\gamma$ until a minimum is reached, where the particles are called Minimum-Ionizing Particles (MIPs). At higher $\beta\gamma$ values there is a relativistic rise, where the energy loss increases until a constant value – the Fermi plateau – is reached. The Bethe-Bloch formula is valid in the region $0.1 < \beta\gamma < 1000$ and can be used for Particle Identification (PID) of charged particles. In figure 2.2 one can see the different energy loss distributions for different particle species in the TPC. The ALEPH collaboration proposed a parameterized Bethe-Bloch formula [BLU 93], which is also used in ALICE. It is given by

$$f(\beta\gamma) = \frac{P_1}{\beta^{P_4}} \cdot \left[P_2 - \beta^{P_4} - \ln\left(P_3 + \frac{1}{(\beta\gamma)^{P_5}}\right) \right], \quad (3.2)$$

where the parameters $P_{1\dots 5}$ depend on the traversed material.



(a)



(b)

Figure 3.2: Energy loss in the TPC versus the rigidity measured in Pb–Pb collisions at $\sqrt{s_{\text{NN}}} = 2.76 \text{ TeV}$. On the top (a) all detected tracks in the TPC and on the bottom (b) only the tracks inside the Bethe-Bloch 3σ -band for ${}^3\text{He}$ are plotted.

In figure 3.2 the energy loss in the TPC is plotted. On the bottom only candidates for ${}^3\text{He}$ are plotted, which deviate at maximum 3σ from the expected value calculated with the Bethe-Bloch formula. In order to reject possible false candidates, the plotted nuclei are matched with ${}^3\text{He}$ candidates identified with TOF also in a 3σ range of the expected value. This preselection is the precondition to investigate the performance of nuclei in the TRD and is made also for deuterons (d), tritons (t) and alpha particles (${}^4\text{He}$).

3.3 Transverse momentum p_T

The magnetic field in the L3 magnet is a homogeneous \vec{B} field in longitudinal direction relative to the detectors. The Lorentz force causes a circular particle trajectory. Therefore, the momentum p of the traversing particles has a longitudinal and a transverse component. The transverse component is:

$$p_T = e \cdot r \cdot B, \quad (3.3)$$

with the elementary charge e , the magnetic induction B and the radius r of the circular particle track. To determine the radius from the measurements in the TRD, a straight line fit (blue line in figure (3.3)) is used. From figure 3.3 the radius is given by:

$$r = \frac{d_{AB}/2}{\sin(\alpha)} \quad (3.4)$$

with $\alpha = \varphi_B - \varphi_A = \arctan\left(\frac{y_B}{x_B}\right) - \arctan\left(\frac{y_A}{x_A}\right)$ (3.5)

and $d_{AB} = \sqrt{(x_B - x_A)^2 + (y_B - y_A)^2} = \sqrt{1 + b^2} \cdot (x_B - x_A)$ (3.6)

with $y_A = a + b \cdot x_A$ $y_B = a + b \cdot x_B$

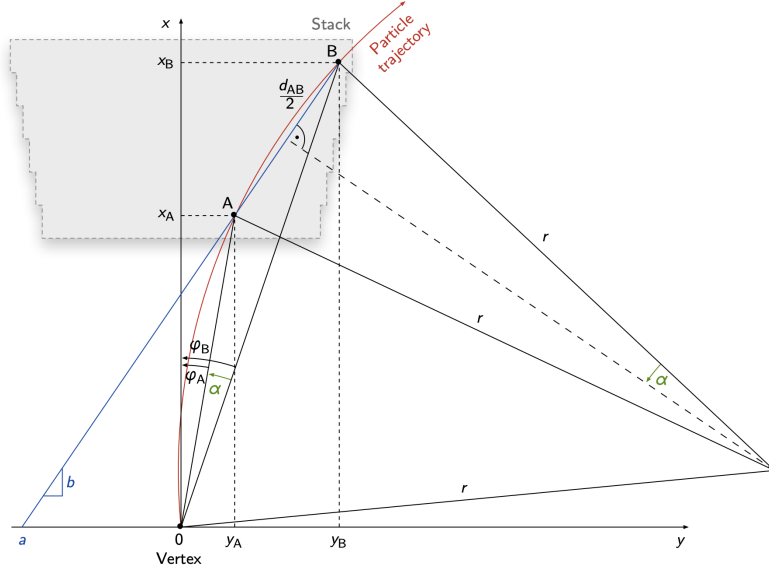


Figure 3.3: Illustration of a straight line fit in the TRD. The parameters a and b are used to calculate the transverse momentum p_T [CUV 09].

For small b^2 the root in (3.6) can be expanded, so the calculation d_{AB} now reads:

$$d'_{AB} = (x_B - x_A) \left(1 + \frac{b^2}{2} \right) \quad (3.7)$$

So, equation (3.4) can be simplified by using geometric approximations

$$\sin(\alpha) \approx \alpha \quad (\text{for small } \alpha) \text{ and} \quad (3.8)$$

$$\arctan(x) \approx x \quad (\text{for small } x). \quad (3.9)$$

to

$$r' = \frac{d'_{AB}}{2 \cdot (\varphi_B - \varphi_A)} \quad (3.10)$$

Using (3.9) and expanding $\alpha = \varphi_B - \varphi_A$ as a Taylor series (3.7) leads to:

$$r'' = c_1 \cdot \frac{\frac{b^2}{2} + 1}{a(b^2 - 1) + a^2 b c_2} \quad (3.11)$$

with

$$c_1 = \frac{x_A x_B}{2} \quad \text{and} \quad c_2 = \frac{x_A + x_B}{x_A x_B}$$

Finally, as the values a and therefore the slope b are small, the squared terms in equation (3.11) vanishes and a simple relation results:

$$r''' = - \frac{c_1}{a} \quad (3.12)$$

Relation (3.12) can be used in (3.13), whereby the transverse momentum p_T is inversely proportional to the distance a to the vertex. A negative charge particle, and thus also the anti-nuclei, has a curvature in the other direction. Therefore, a is positive along the y-axis in figure (3.3) and the transverse momentum is negative per definition.

Using formula (3.12) the transverse momentum p_T finally leads to:

$$p_T = - e \cdot \frac{c_1}{a} \cdot B = - e \cdot \frac{x_A x_B}{2a} \cdot B \quad (3.13)$$

3.4 Charge deposition in the TRD

As described in the previous sections, traversing particles interact with the electrons of the gas atoms in the drift region, which causes excitation or ionisation, if the energy transfer is higher than the ionization potential. The number of electrons of the produced clusters measured by a TRD chamber is proportional to the energy deposition. Therefore, the energy deposition can be described by the deposited charge Q_s per tracklet. This signal is translated into an 8-bit value via a transformation function, i.e. the charge deposition is represented by numbers 0–255 in arbitrary units to reduce storage capacity. This transformation function, which is a linear function for this dataset, is stored in a Look-Up Table (LUT) in the TRAP chip in the FEE. Finally, the information on the charge deposition per track are the mean $\langle Q_s \rangle$ values of the contributing tracklets:

$$\langle Q_s \rangle = \frac{1}{N} \sum_{i=0}^N Q_{s,i} \quad (3.14)$$

with the number of contributing tracklets N ($N = 1 - 6$). The mean charge deposition distribution over p_T/Z , where Z is the atomic number, is illustrated in figure 3.4. One can see most of the charge deposition is in low $\langle Q_s \rangle$ range.

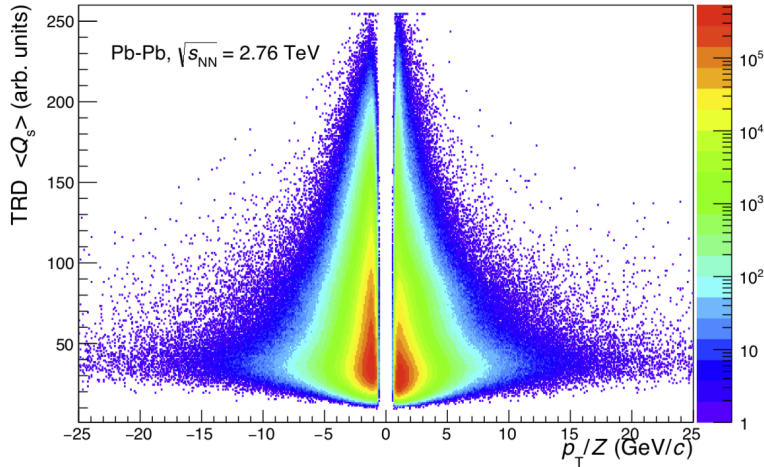


Figure 3.4: Mean charge deposition distribution of all tracks in the TRD.

To analyse the behavior of light nuclei in the TRD, they were preselected with the TPC and TOF Particle IDentification (PID) information, which is presented in section 3.2. So, only the TRD mean charge deposition distribution of the nuclei are plotted, which are identified both in TPC and TOF. This is separately done for deuterons, tritons, ${}^3\text{He}$ and

alpha particles ${}^4\text{He}$. In case of deuterons and tritons, there was an additional preselection on TPC rigidity data to reduce contamination from other tracks:

$ \text{TPCnSigma} < 3\sigma$		
Only $ \text{TPCnSigma} < 3\sigma$		
Deuterons	$ p/z < 1.4 \text{ GeV}/c$	$ p/z < 1.7 \text{ GeV}/c$
Tritons	$ p/z < 1.7 \text{ GeV}/c$	$ p/z < 2.0 \text{ GeV}/c$

Table 3.1: Different rigidity cuts for the analysis of deuterons and tritons.

Figure 3.5 illustrates the mean charge deposition distribution of these light nuclei. In high-energy collision experiments both, particles and their antiparticles, the same amount is expected to be produced. The different yield between the measured particles and anti-

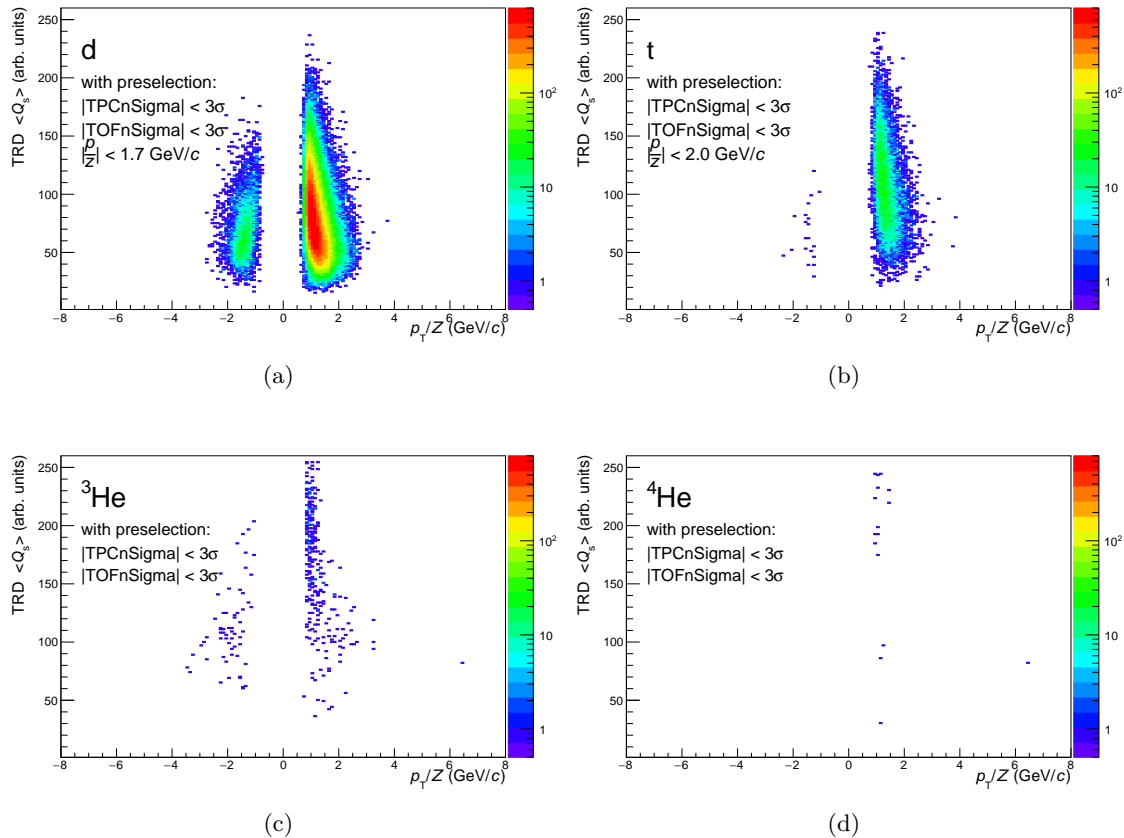


Figure 3.5: Mean charge deposition distribution of deuteron (a), triton (b), ${}^3\text{He}$ (c) and alpha particles (d) in the TRD. All tracks are preselected with the Bethe Bloch 3σ -band on TPC energy loss and 3σ on TOF β -momentum distribution information.

particles is caused dominantly by two main effects. If an anti-particle collides with its counterpart, e.g. a particle in the detector material, other particles will be produced under conservation of energy and momentum. This process is called annihilation, which reduces the yield of antiparticles. Furthermore, a collision of particles with the detector material produces knock-out particles, which increases the yield of positive charge nuclei.

In the following figure 3.6 the projection of each charge deposition distribution in figure 3.5 to the y-axis is shown. For a better comparison of the different distributions, the yields has been normalized. In this representation the nuclei and their anti-nuclei are not distinguishable any more.

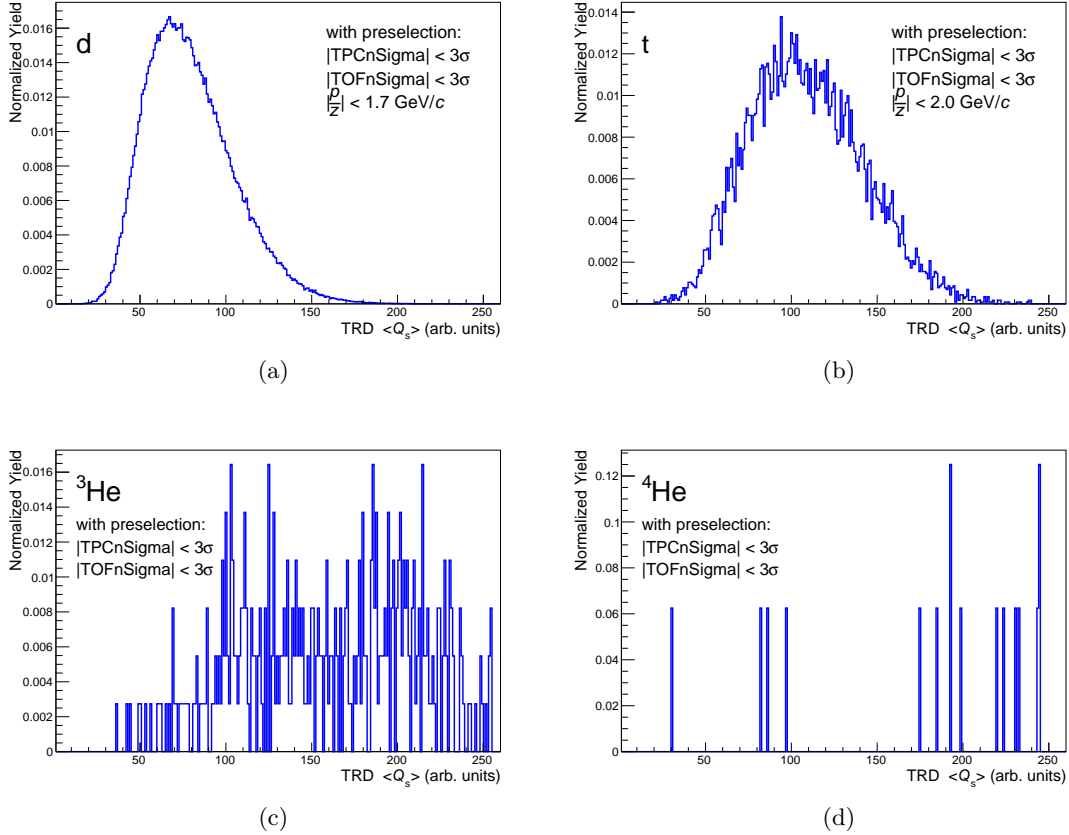


Figure 3.6: Normalization and y-axis projection of the plots in figure 3.5.

For deuterons and tritons a relative clear distribution is seen. This is caused by the large number of identified d and t of 254.2×10^3 respectively 11.6×10^3 candidates. However, the small yields of ${}^3\text{He}$ and ${}^4\text{He}$, 365 respectively 16 candidates, causes a distribution, where the means have large uncertainties. For a better description of the distribution more statistics is needed. Without the preselection of the TOF detector in addition to TPC PID, the yields of ${}^3\text{He}$ and ${}^4\text{He}$ are large enough to populate a more precise charge

deposition distribution. This is shown in figure 3.7 and also used in figure 4.2 and section 4.2, which discusses the results of the feasibility study in the following chapter.

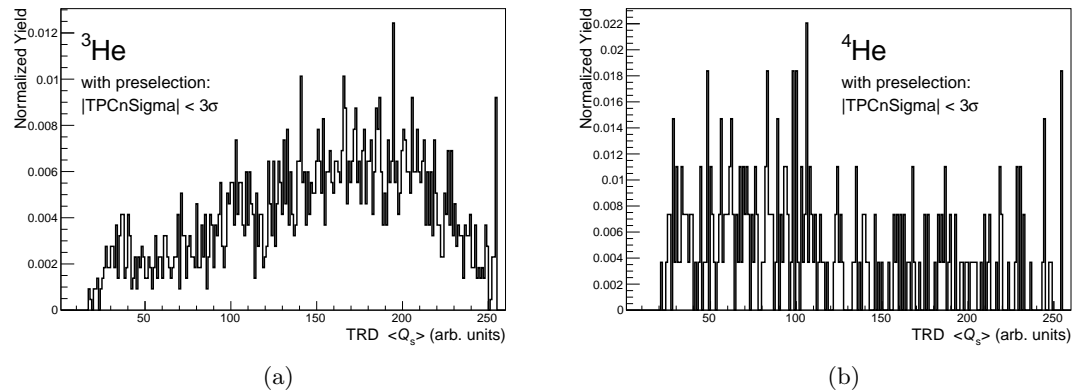


Figure 3.7: Normalization and y-axis projection of ${}^3\text{He}$ (a) and alpha particles ${}^4\text{He}$ (b) which are identified in the TPC only.

4 Feasibility Study on Real Data

In this chapter the concept of the nuclei trigger will be explained first. After that, the study using real data, which were introduced in section 3.1, and its results will be presented.

4.1 Trigger concept

In section 3.4 the mean charge deposition in the TRD is discussed. In figure 3.4 one can see an accumulation of entries at lower $\langle Q_s \rangle$ values. When light nuclei are distinguished from all other particles, their distribution is centered at higher $\langle Q_s \rangle$ values, as shown in figure 4.1. The basic idea of a nuclei trigger is to implement a threshold on this observable. With this threshold only events will be stored, where at least one track is measured with a $\langle Q_s \rangle$ value above the threshold, which in term will increase the possibility to measure light nuclei candidates.

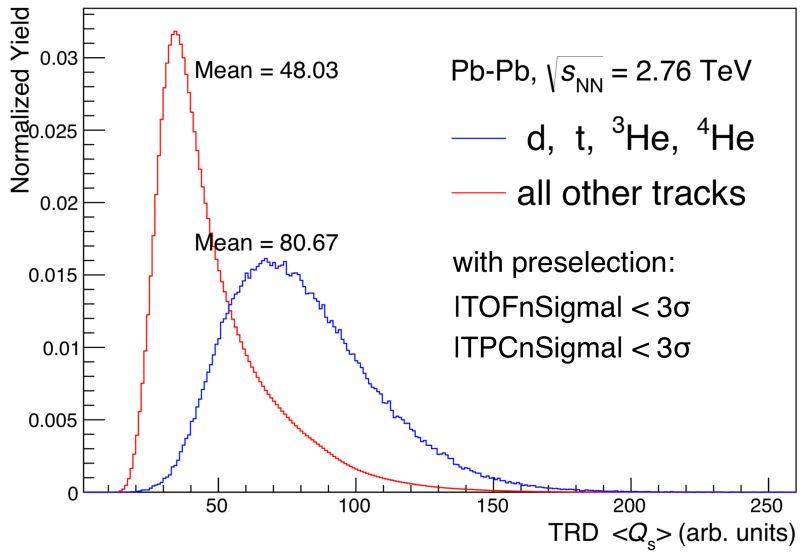


Figure 4.1: Mean charge deposition distribution of all tracks in the TRD. Light nuclei are preselected with TPC and TOF.

At first the $Z = 2$ nuclei ${}^3\text{He}$ and ${}^4\text{He}$ were investigated. Because of factor Z^2 in the Bethe Bloch formula (3.1) these nuclei deposit four times more charge than nuclei with a charge

number of $Z = 1$. In the following figure 4.2 the mean charge deposition distribution of the light nuclei d, t, ^3He and ^4He is shown separately. To compare light nuclei with other particles this procedure was also applied to electrons, pions, protons and kaons, which are the most abundant particles in this dataset. Table 4.1 demonstrates that these particles deposit charge in rather the same $\langle Q_s \rangle$ range. Therefore, all other tracks than the light nuclei are plotted as one mean charge deposition distribution (the red curve in figure 4.1 and 4.2). The distribution can be fitted by a modified Landau-Gaussian convolution

$$e^{\kappa x} \text{Landau}(x) * \text{Gaussian}(x), \quad (4.1)$$

where the Landau distribution is weighted by an exponential dampening [ALI 17][LU 13]. In addition to enhanced $Z = 2$ nuclei one can also see an enhancement at high $\langle Q_s \rangle$ values for deuterons and tritons. Therefore a threshold on a $\langle Q_s \rangle$ value will increase also the statistics of d and t. Such a trigger decision can be done at trigger level-1 in the GTU.

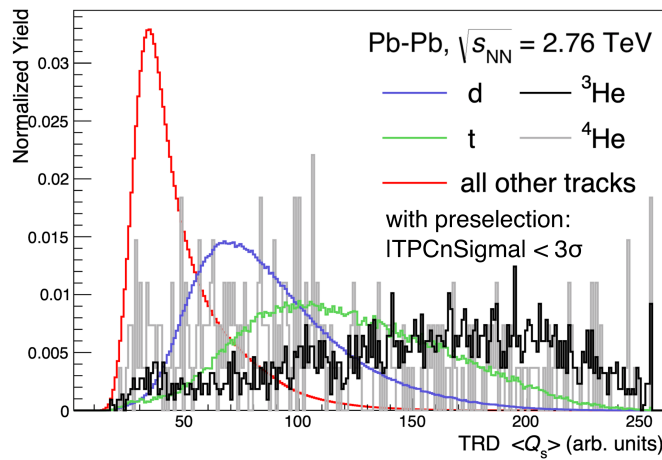


Figure 4.2: Mean charge deposition distribution of all tracks identified by TPC only.
d, t, ^3He and ^4He are shown separately.

Particle	$\langle Q_s \rangle$ (arb. units)	Particle	$\langle Q_s \rangle$ (arb. units)
Electron	52.13	Deuteron	79.26
Pion	46.43	Triton	108.90
Kaon	46.97	${}^3\text{He}$	158.90
Proton	49.69	${}^4\text{He}$	180.10

Table 4.1: Average values $\langle Q_s \rangle$ on mean charge deposition distributions of different particles preselected with TPC and TOF.

The goal is now to investigate the impact of a nuclei trigger and to determine an optimal $\langle Q_s \rangle$ value for a threshold. Such a nuclei trigger will not store most of the candidates of

protons, pions, electrons and kaons, as they have a mean charge deposition distribution centered at lower $\langle Q_s \rangle$ values (see figure 4.1). To investigate the impact of the threshold three quantities will be introduced in the next section 4.1.1.

4.1.1 Purity, trigger efficiency, rejection factor

The main part of the feasibility study is the comparison of different thresholds with the help of the three quantities (4.2), (4.3) and (4.4). Purity is the ratio between the number of nuclei d, t, ^3He and ^4He passing the threshold X and the number of all other particles passing the same threshold. If only an individual nucleus is investigated, all other particles except this nucleus are in the denominator of the ratio. Because of the enhancement of light nuclei at high $\langle Q_s \rangle$ values an increasing purity is expected. The trigger efficiency reveals the amount of light nuclei passing the threshold divided by the yield of the same nuclei in the dataset without a nuclei trigger. The so-called rejection factor is the ratio of all other particles than d, t, ^3He and ^4He passing also the threshold to the amount of these particles in the dataset without a nuclei trigger.

$$\text{Purity} = \frac{N_{\text{nuclei}}(\langle Q_s \rangle > X)}{N_{\text{else}}(\langle Q_s \rangle > X)} \quad (4.2)$$

$$\text{Trigger efficiency} = \frac{N_{\text{nuclei}}(\langle Q_s \rangle > X)}{N_{\text{nuclei}}(\text{without trigger})} \quad (4.3)$$

$$\text{Rejection factor} = \frac{N_{\text{else}}(\langle Q_s \rangle > X)}{N_{\text{else}}(\text{without trigger})} \quad (4.4)$$

4.2 Results

An issue in the determination of a suitable threshold is to achieve a high purity and efficiency, but not to reject too many particles, which could be used for other physics analyses. The approach in the following is to investigate the behavior of these three observables for different $\langle Q_s \rangle$ thresholds in steps of 10 arbitrary units from 0 to 250. The presented results in the following are the results of the study on nuclei preselected with TPC and TOF. However, this feasibility study is based on track level decisions, what means, that with a determined threshold none of the identified particles with a $\langle Q_s \rangle$ value below that threshold would be allowed. In comparison the suggested concept of a nuclei trigger still allows particles with a $\langle Q_s \rangle$ value below a threshold, because only one track with a $\langle Q_s \rangle$ value above the threshold is required to store one whole event. Therefore, real data taking processes with an implemented nuclei trigger on event level will be obtain a

slightly lower purity. However, the procedure used in this study nevertheless allows for an appropriate evaluation of the feasibility of a nuclei trigger.

4.2.1 Purity

In figure 4.3 (a) one can see that the purity increases with increasing $\langle Q_s \rangle$ thresholds, up to $\langle Q_s \rangle \approx 120$ a.u. In the range of 120 a.u. $< \langle Q_s \rangle < 190$ a.u. there is a plateau, where no further increase is seen. At values higher than 190 a.u. the purity increases again, however with higher uncertainties because of low statistics. The right plot (b) reveals the purity peaks for different $\langle Q_s \rangle$ thresholds for individual nuclei. An explanation of the plateau is decreasing purity for deuterons at $\langle Q_s \rangle > 120$ a.u., where the purities for tritons, ^3He and alphas increases.

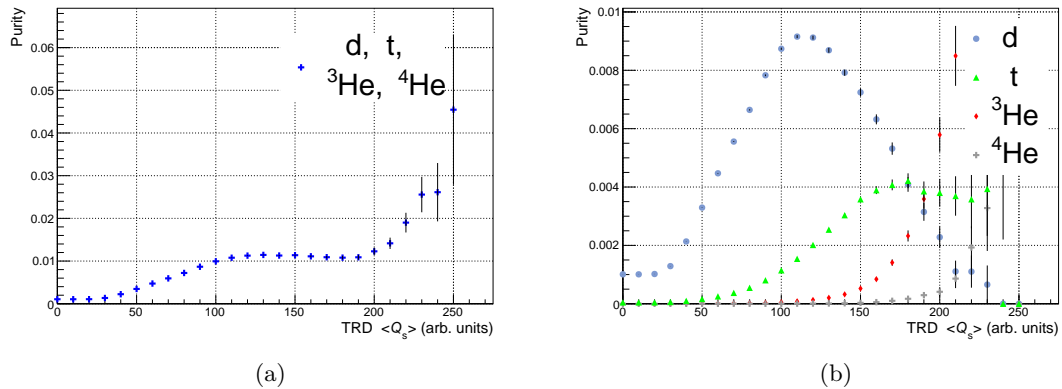


Figure 4.3: The purity for light nuclei for several $\langle Q_s \rangle$ thresholds is plotted on the left side (a) and separated for individual nuclei on the right (b).

The higher the threshold is the more particles will be rejected. Due to the constant behavior on the purity of light nuclei in the range of 120 to 190, the following results on purities are presented for an assumed threshold of $\langle Q_s \rangle > 100$ in arbitrary units:

	Without trigger	$\langle Q_s \rangle > 100$ arb. units
d	$(1008.2 \pm 2.0) \times 10^{-6}$	$(8738.4 \pm 38.6) \times 10^{-6}$
t	$(46.1 \pm 0.4) \times 10^{-6}$	$(1145.4 \pm 13.9) \times 10^{-6}$
^3He	$(1.45 \pm 0.08) \times 10^{-6}$	$(53.7 \pm 3.0) \times 10^{-6}$
^4He	$(0.06 \pm 0.02) \times 10^{-6}$	$(2.0 \pm 0.6) \times 10^{-6}$
d, t, ^3He & ^4He	$(1055.8 \pm 2.0) \times 10^{-6}$	$(9939.5 \pm 41.2) \times 10^{-6}$

Table 4.2: Purity results for light nuclei preselected with TPC and TOF. The right column represents the results for an assumed threshold at $\langle Q_s \rangle > 100$ arb. units.

For these nuclei one can see an increase of the purity with an implemented nuclei trigger, especially for $Z = 2$ nuclei ^3He and ^4He . It shows an increase by a factor of 37, respectively 32, for ^3He and ^4He .

4.2.2 Trigger efficiency

In figure 4.4 one can see the trigger efficiency for light nuclei. On the left plot (a) this observable is plotted for d, t, ^3He and ^4He taken together. The higher the threshold is set the more nuclei will be also rejected and therefore the trigger efficiency decreases towards higher thresholds. Because deuterons are dominating, as shown in table 4.3, and their low mean charge depositions in the TRD, the values are decreasing fast. The right plot (b) represents the trigger efficiency for separate nuclei. The large uncertainties for alpha particles are caused by the small number of measured candidates. For $Z = 2$ particles a threshold of $\langle Q_s \rangle > 150$ arbitrary units seems to be feasible with trigger efficiencies still over 50% and higher purities than with $\langle Q_s \rangle > 100$ arbitrary units. However, the number of rejected other particles for such a high threshold would be too high in this case. This will be discussed in the next subsection 4.2.3.

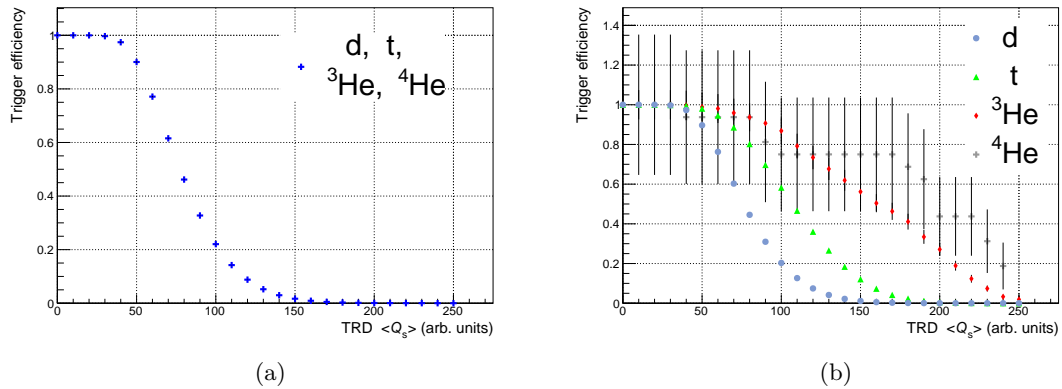


Figure 4.4: The trigger efficiency for all light nuclei is plotted on the left side (a) and for individual nuclei on the right (b).

	N_{nuclei} Without trigger	N_{nuclei} $\langle Q_s \rangle > 100 \text{ a.u.}$	Trigger efficiency $\langle Q_s \rangle > 100 \text{ a.u.}$
d	254174 ± 504.2	51602 ± 227.2	$(20.30 \pm 0.09) \%$
t	11610 ± 107.8	6764 ± 82.2	$(58.26 \pm 0.89) \%$
${}^3\text{He}$	365 ± 19.1	317 ± 17.8	$(86.85 \pm 6.67) \%$
${}^4\text{He}$	16 ± 4	12 ± 3.5	$(75.00 \pm 28.64) \%$
d, t, ${}^3\text{He}$ & ${}^4\text{He}$	266164 ± 515.9	58695 ± 242.3	$(20.30 \pm 0.10) \%$

Table 4.3: Trigger efficiency results for light nuclei preselected with TPC and TOF. The two right columns represent the results for an assumed threshold at $\langle Q_s \rangle > 100$ a.u.

4.2.3 Rejection factor

The rejection factor, defined in formula (4.4), is an important observable for other physics analyses, where e.g. a huge number of electrons are necessary. A high threshold would increase the purity of light nuclei and therefore the probability to measure rare particles like an anti-alpha. However, it would dramatically decrease the amount of other particles, because of their preferred mean charge deposition at low $\langle Q_s \rangle$ values. The dashed red line in 4.5 represents a trigger rejection of 1/1000, meaning that only 0.1 % of the identified events will be stored and all other candidates rejected. The trigger rejection should not be below that value.

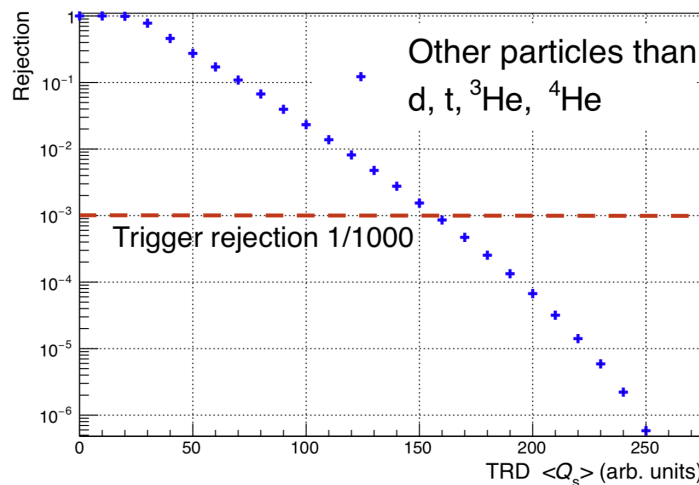


Figure 4.5: Ratio of other particles than d, t, ${}^3\text{He}$, ${}^4\text{He}$ which pass the threshold over the amount of these particles without a threshold.

In the case of an assumed threshold of $\langle Q_s \rangle > 100$ a.u. on track level the rejection factor would be (2.324 ± 0.001) % which is equal to approximately 1/42. As discussed in section 4.1 the implementation of a nuclei trigger will be on event level and therefore particles with $\langle Q_s \rangle$ values below the threshold will be stored. This causes an increase of the numerator in formula (4.4) and still allows for high statistics for other physics analyses. The quantitative description of the increase is depending on the multiplicity of the collision systems.

4.3 p_T dependence

To investigate a possible transverse momentum dependence it is essential to recalculate the results for several p_T slices, which are shown in figure 4.6. For all three observables, purity, trigger efficiency and rejection factor, enhanced results for low p_T range are visible, especially for $p_T < 2$ GeV/c. Therefore $p_T < 2$ GeV/c as an additional condition to a $\langle Q_s \rangle$ threshold is suggested for a nuclei trigger.

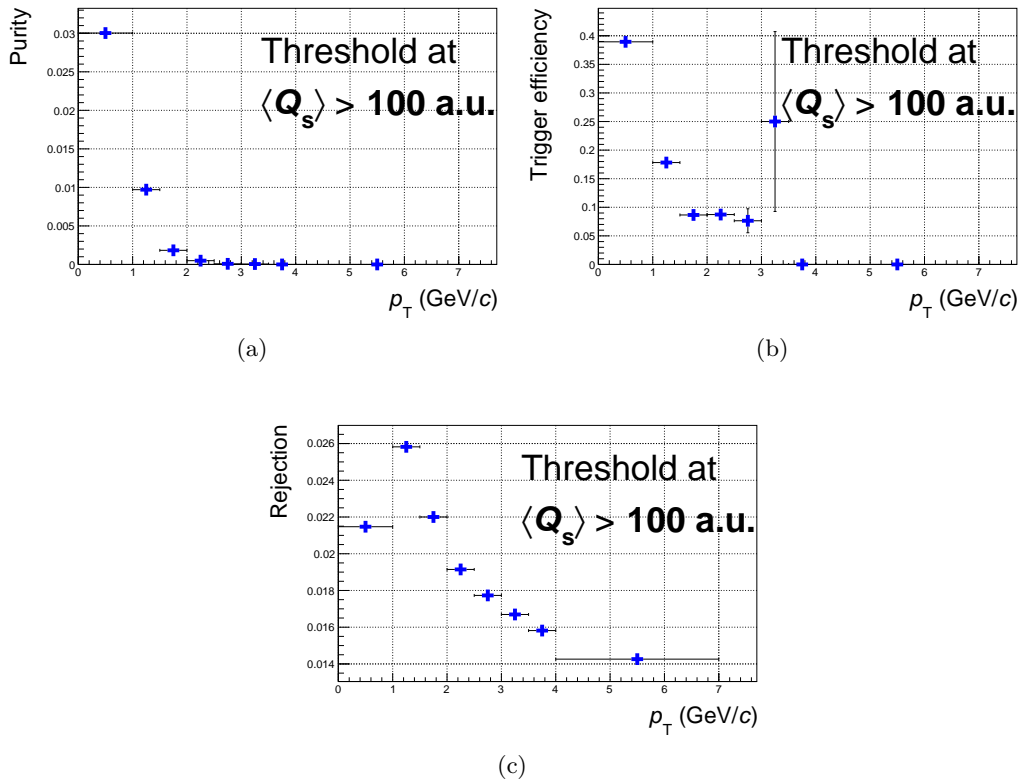


Figure 4.6: Transverse momentum dependence on purity (a), trigger efficiency (b) and rejection factor (c) for light nuclei (d , t , ${}^3\text{He}$, & ${}^4\text{He}$) preselected with TPC and TOF at an assumed threshold of $\langle Q_s \rangle > 100$ a.u.

4.4 Conclusion

To quantify the impact of a nuclei trigger three observables were introduced in section 4.1.1 – purity, trigger efficiency and rejection factor. The majority of identified particles deposit charge in the range of $\langle Q_s \rangle \approx 48$. The average values on $\langle Q_s \rangle$ distributions for nuclei can be found in table 4.1. The impact on the observables was investigated for several $\langle Q_s \rangle$ threshold in steps of 10. With a focus on maximizing the statistics of deuterons a threshold in the range of $110 < \langle Q_s \rangle < 120$ would be ideal because of the highest purity. Nevertheless, an optimal threshold with a focus on tritons would be in the range of $170 < \langle Q_s \rangle < 190$ and with a focus on $Z = 2$ particles in an even higher $\langle Q_s \rangle$ range, again just because of the highest purity. However, the higher the threshold is set the lower are trigger efficiency and rejection factor (see figures 4.4 and 4.5). To determine a suitable threshold one also has to consider that good statistics for other physics analyses, where e.g. a huge amount of electrons are necessary, has to be ensured. Therefore, a nuclei trigger should not reject too many other particles.

The results demonstrate the feasibility of a nuclei trigger. To consider the conditions a threshold in the range of $\langle Q_s \rangle \approx 100$ is suggested. A further investigation of a possible p_T dependence reveals enhanced results in low p_T range. Therefore, an additional threshold on transverse momentum of $p_T < 2 \text{ GeV}/c$ is suggested. A final step will be to implement the trigger and to test the impact in a test run. To ensure the consideration of other physics cases a modification on the look-up table is required. This will be discussed in the following chapter 5.

5 Trigger Tests

As the feasibility studies turned out to be successful, the next step is to test such a trigger under real conditions. As described in previous chapters, the feasibility of a nuclei trigger is studied with data on Pb–Pb collisions at $\sqrt{s_{\text{NN}}} = 2.76$ TeV. However, the nuclei trigger will be applied to data on Pb–p and p–Pb collisions at $\sqrt{s_{\text{NN}}} = 8.16$ TeV in 2016. One challenge for this test runs is to implement the nuclei trigger (HNU) together with a single electron trigger (HSE), a quarkonia trigger (HQU) and a jet trigger (HJT), since only one is existing on the electronics. Therefore, the look-up table has to be modified. To enable this a ROOT-macro `AliTRDcreateLUT.C` was created, which translates an arbitrary function into a look-up table [BRU 16].

5.1 Look-up table

A look-up table (LUT) is directly implemented in a TRAP chip, which transfers the measured raw data in a TRD chamber into an 8-bit value (0-255). For the Pb–Pb dataset, used for this feasibility study, a linear transformation function was used in the LUT. In figure 5.1 the green function represents the linear LUT. A measured mean charge deposition above approximately 13000 ADC-counts has been translated into a $\langle Q_s \rangle$ value of 255.

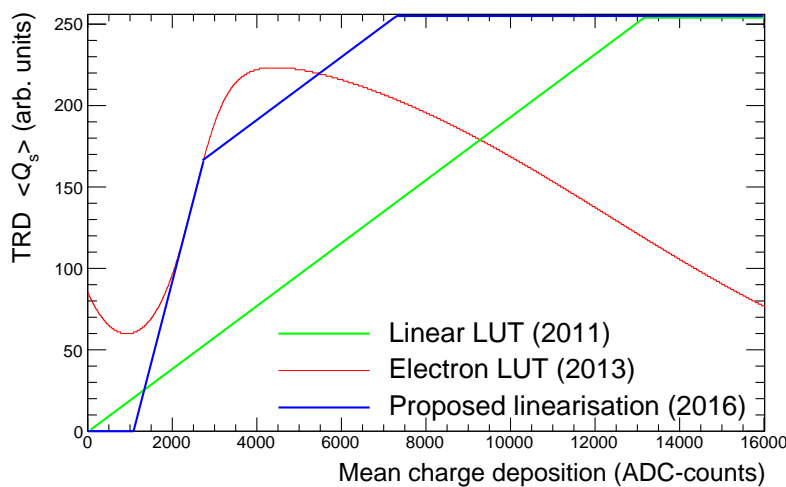


Figure 5.1: Shapes of different used look-up tables.

The red function represents a LUT created for triggering on electrons in 2013 [HE β 11]. An advantage is the high slope in the range of deposited charge below approximately 2750 ADC-counts, which ensures a high $\langle Q_s \rangle$ resolution to discriminate electrons from other particles. However, a disadvantage is that the electron LUT allows more than one raw charge deposition value for one $\langle Q_s \rangle$ value. Therefore, these stored $\langle Q_s \rangle$ values are indistinguishable. To implement a nuclei trigger together with triggers on electrons the blue function in figure 5.1 is proposed as a new LUT. For low $\langle Q_s \rangle$ range it has the same slope as the the electron LUT at 2750 ADC-counts and the same slope as the linear LUT used in 2011 for values above 2750 ADC-counts. Deposited charges of above approximately 7250 ADC-counts will be translated into a $\langle Q_s \rangle$ value of 255. Because of the implementation of that new look-up table the suggested thresholds for a nuclei trigger has other values, that can be easily translate from the linear LUT.

5.2 Settings for TRD triggers

For data on Pb–p and p–Pb collisions at $\sqrt{s_{\text{NN}}} = 8.16$ TeV the thresholds in table 5.1 are implemented as level-1 triggers. To compare the $\langle Q_s \rangle$ thresholds with the suggested thresholds in this thesis, the values can be translate from the LUT of 2016 (blue function in figure 5.1) into the linear LUT of 2011 (the green function in figure 5.1). The final $\langle Q_s \rangle$ threshold for the nuclei trigger was $\langle Q_s \rangle > 207$ with the new LUT, which is equal to $\langle Q_s \rangle \gtrsim 93$ with the linear LUT. The determination of a lower threshold than the suggested one causes less rejection of electrons and other particles to enable good statistics for other physics analyses.

Trigger	N_{tracks}	$\langle Q_s \rangle$	p_T
HNU		> 207	$< 2 \text{ GeV}/c$
HQU		> 135	$> 2 \text{ GeV}/c$
HSE		> 120	$> 3 \text{ GeV}/c$
HJT	≥ 3		$> 3 \text{ GeV}/c$

Table 5.1: Thresholds for the implemented nuclei trigger (HNU), quarkonia trigger (HQU), single electron trigger (HSE) and jet trigger (HJT) in Pb–p and p–Pb test runs at $\sqrt{s_{\text{NN}}} = 8.16$ TeV [DOE 17].

5.3 First look into new data

The first results for the Pb–p and p–Pb test runs LHC16s (Pb–p) and LHC16r (p–Pb) are shown in the following. The total number of stored minimum bias events are 4.9×10^7 , respectively 6.4×10^7 , in these datasets [DOE 17]. The inspection rate of the level-0 trigger is 10 kHz and the number of fired triggers and its readout rates are presented in table 5.2.

Readout rates		$N_{\text{fired triggers}}$
HNU	19 Hz	3,544,049
HQU	42 Hz	8,184,440
HSE	40 Hz	7,700,510
HJT	2 Hz	289,433
Total	≈ 100 Hz	

Table 5.2: Readout rates and number of fired triggers in data on Pb–p and p–Pb collisions at $\sqrt{s_{\text{NN}}} = 8.16$ TeV for 0.81 nb^{-1} inspected luminosity. The inspection rate from trigger level-0 is 10 kHz [DOE 17].

In table 5.2 one can see, that approximately 3.5×10^6 events have been stored, which fulfill the conditions of the nuclei trigger HNU. Due to an enhancement of light nuclei one can expect a higher number of measured deuterons, tritons, ${}^3\text{He}$, alphas and their anti-particles. In figure 5.2 all measured negatively charged particles are shown, where the energy loss in the TPC in dependence on rigidity is plotted. The red lines represent the Bethe-Bloch curves for the expected particles. With the particle identification ability of the TOF detector in addition to TPC–PID informations several ${}^3\text{He}$ and four ${}^4\text{He}$ candidates are identified. So, anti-alphas have been observed for the first time in p–Pb collisions with the ALICE detector.

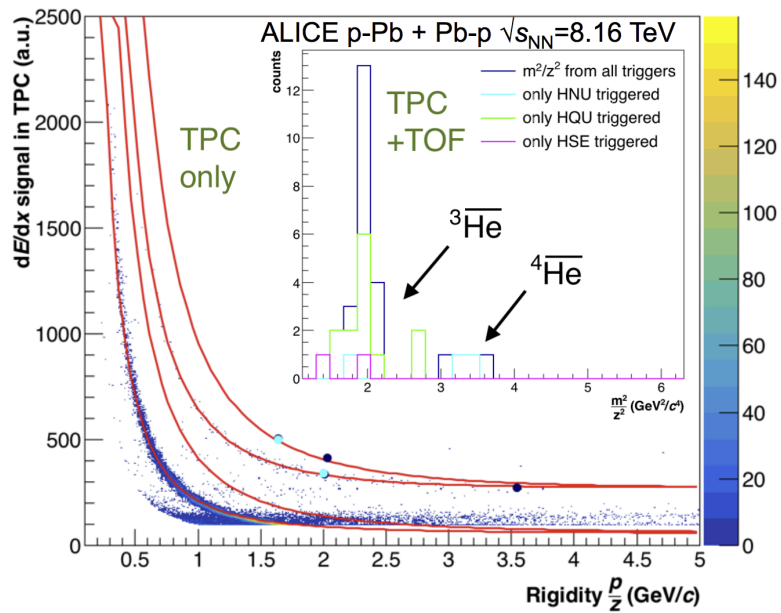


Figure 5.2: Results from the successful trigger campaign in the 8.16 TeV Pb–p and p–Pb data taking in 2016. Only negative charged particles are shown [DOE 17].

6 Summary and Outlook

In high-energy physics the understanding of the production mechanism of light nuclei is a topic of high interest. However, the production rates of light nuclei are small, what limits the significance of results of several physics analyses on light nuclei. One example, where a lack of statistics is an issue, is the "hypertriton lifetime puzzle". The hypertriton ${}^3_{\Lambda}\text{H}$ is a bound system of a proton, a neutron and a Λ -baryon with a theoretical predicted lifetime of 256 ps [KAM 98], which is close to the lifetime of a free lambda Λ (263.2 ps [PDG 14]). To study the hypertriton only its decay products can be measured in the ALICE–TPC, TRD and TOF, because of its short lifetime and decay length ($c\tau \approx 7$ cm). In both, the two-body and the three-body mesonic decay, light nuclei are decay products. However, recent results on Pb–Pb collisions show a significant shorter lifetime than the theoretical predicted lifetime. This results have to be compared with results on p–Pb and pp collisions. Therefore, a nuclei trigger is required in order to enhance the amount of light nuclei.

In this thesis the feasibility of a nuclei trigger using the ALICE–TRD was studied. Because of the fast trigger decision ability of 7.7 μs after initial collisions, the TRD is appropriate to function as a trigger detector on trigger level-1. A goal at first was to investigate the impact of such a trigger on offline data. The examined dataset was on Pb–Pb collisions at $\sqrt{s_{\text{NN}}} = 2.76$ TeV measured by ALICE in 2011. A central observable is the mean charge deposition $\langle Q_s \rangle$ of a traversing particle, measured by at least 4 of 6 chambers in a TRD stack. The measured raw value is translated into an 8-bit value (0–255) with the usage of a look-up table (LUT) directly available in the FEE. The TRD mean charge deposition distribution shown in figure 3.4 contains only information on the amount of deposited charge of all tracks in dependence on transverse momentum and the atomic number of the particles. To investigate separately the behavior on the charge deposition of identified particles, one has to use the TPC and the TOF detector to preselect particles and thereby nuclei. The mean charge deposition distribution of deuterons, tritons, ${}^3\text{He}$ and alphas reveals an enhancement at high $\langle Q_s \rangle$ values for these nuclei. The idea of a nuclei trigger is therefore to implement a threshold on this observable and to store only events where at least one track is detected with a mean charge deposition above that threshold.

To study the impact of such a nuclei trigger three quantities namely purity, trigger efficiency and rejection factor were introduced. Then the impact on these observables was investigated for several $\langle Q_s \rangle$ thresholds in steps of 10. The goal was finally to determine a

suitable threshold to ensure on one hand an increased amount of identified light nuclei and on the other hand not to reject too many electrons and other particles of interest for other physics analyses. In addition to a $\langle Q_s \rangle$ threshold the dependence on transverse momentum was investigated. Due to promising results of the feasibility study a $\langle Q_s \rangle$ threshold in the range of $\langle Q_s \rangle \approx 100$ and a threshold on transverse momentum of $p_T < 2 \text{ GeV}/c$ are suggested.

As a final step, the nuclei trigger had to be tested under real conditions. The nuclei trigger had to be implemented together with a quarkonia trigger, a single electron trigger and a jet trigger in Pb–p and p–Pb test runs at $\sqrt{s_{\text{NN}}} = 8.16 \text{ TeV}$. This requires a modification of the linear LUT used for Pb–Pb collisions at $\sqrt{s_{\text{NN}}} = 2.76 \text{ TeV}$ in 2011. For this new LUT (represented as blue function in figure 5.1) the suggested $\langle Q_s \rangle$ threshold of a nuclei trigger had to be translated from the linear LUT (see section 5.2). The final thresholds for a nuclei trigger determined this way were $\langle Q_s \rangle > 207$ and $p_T < 2 \text{ GeV}/c$. A first look into the results demonstrate the success of that trigger campaign. For the first time anti-alphas were observed with the ALICE detector in p–Pb/Pb–p collisions.

A full analysis of this dataset with respect to light nuclei and the hypertriton is in preparation. To study the hypertriton properties one has to investigate both mesonic decay modes, i.e. the two-body and the three-body decay mode. Also the first observation of an anti-alpha has to be confirmed. After the implementation of a nuclei trigger in p–Pb collisions systems the nuclei trigger was implemented for pp collisions at $\sqrt{s} = 13 \text{ TeV}$. This dataset also has to be studied. With a 10 kHz inspection rate 9×10^{10} events are supposed to be inspected and therefore a significant amount of light nuclei are expected.

Bibliography

- [ALI 99] ALICE Collaboration, *Technical Design Report of the Photon Spectrometer (PHOS)*,
CERN / LHCC 99-4; ALICE TDR 2, 1999.
- [ALI 00] ALICE Collaboration, *Technical Design Report of the Time Projection Chamber*,
CERN-LHCC-2000-001; CERN-OPEN-2000-183; ALICE-TDR-7, 2000.
- [ALI 02] ALICE Collaboration, *Technical Design Report of the Time of Flight System*,
CERN-LHCC-2002-016; ALICE-TDR-8-add-1, 2002.
- [ALI 04] ALICE Collaboration, *Technical Design Report on Forward Detectors: FMD, T0
and V0*,
CERN-LHCC-2004-025; ALICE-TDR-011, 2004.
- [ALI 08] ALICE Collaboration, *The ALICE experiment at the CERN LHC*,
JINST 3 S08002, 2008.
- [ALI 10] J. Alme et al., *The ALICE TPC, a large 3-dimensional tracking device with fast
readout for ultra-high multiplicity events*,
Nucl. Instrum. Meth. A622 (2010) 316–367, arXiv:1001.1950 [physics.ins-det].
- [ALI 14] ALICE Collaboration, *Performance of the ALICE Experiment at the CERN
LHC*,
Int. J. Mod. Phys. A 29, 1430044, arXiv:1402.4476, 2014.
- [ALI 16] ALICE Collaboration, ${}^3\Lambda H$ and ${}^3\bar{\Lambda} \bar{H}$ production in Pb–Pb collisions at $\sqrt{s_{NN}} =$
2.76 TeV,
Phys. Lett. B 745, 360–372, 2016.
- [ALI 17] ALICE Collaboration, *The ALICE Transition Radiation Detector: construction,
operation, and performance*,
arXiv:1709.02743v2 [physics.ins-det], 2017.
- [ALI WIK] <https://alice-wiki.gsi.de/cgi-bin/view/Data/ALICEDataAtGSI>
- [BET 32] H. Bethe, *Zur Theorie des Durchgangs schneller Korpuskularstrahlen durch Ma-
terie*,
Annalen der Physik, 397:325, 1930.

- [BLO 33] F. Bloch, *Zur Bremsung rasch bewegter Teilchen beim Durchgang durch Materie*, Annalen der Physik, 16:285, 1933.
- [BLU 93] W. Blum, L. Rolandi, *Particle Detection with Drift Chambers*, Springer, 1993
- [PBM 03] P. Braun-Munzinger, K. Redlich, J. Stachel, *Particle Production in Heavy Ion Collisions*, arXiv:nucl-th/0304013v1, 2003.
- [BRU 16] B. Brudnyj, J. Klein, `AliTRDcreateLUT.C` on GitHub, 2016.
- [CUV 09] J. de Cuveland, *A Track Reconstructing Low-latency Trigger Processor for High-energy Physics*, PhD thesis. University of Heidelberg, 2009.
- [DOE 17] B. Dönigus, *TRD status report*, ALICE WEEK March 2017.
- [GAL 18] A. Gal, H. Garcilazo, *Revisiting the ${}^3\Lambda H$ lifetime*, arXiv:1811.03842v1 [nucl-th], 2018.
- [GSI 15] N. Löher, TU Darmstadt, 2015
- [HEß 11] B. A. Heß, *Online Electron Identification for Triggering with the ALICE Transition Radiation Detector*, Diploma thesis. University of Heidelberg, 2011.
- [KAM 98] W. Glöckle, J. Golak, H. Kamada, K. Miyagawa, H. Witała, π -mesonic decay of the hypertriton, Phys. Rev. C 57, 1595, 1998.
- [KLE 11] J. Klein, *Triggering with the ALICE TRD*, arXiv:1112.5110v1 [nucl-ex], 2011.
- [LOE 18] N. Löher, *Search for exotic bound states and measurement of the (anti-)alpha production yield in Pb–Pb collisions with ALICE at the LHC (CERN)*, Dissertation, 2018.
- [LU 13] X.-G. Lu, *Energy Loss Signals in the ALICE TRD*, Nucl. Instrm. Meth. A706, 16-19, arXiv:1204.1218 [physics.ins-det], 2013.
- [PDG 14] Particle Data Group, *Particle Physics Booklet*, July 2014.
- [RAP 14] C. Rappold et al., *On the measured lifetime of light hypernuclei ${}^3\Lambda H$ and ${}^4\Lambda H$* , Phys. Lett. B 728, 543-548, 2014.

[TRO 18] S. Trogolo, *Addressing the (anti-)hypertriton lifetime puzzle with ALICE at the LHC*,
Talk at Quark Matter 2018.

Danksagung

Zunächst möchte ich Professor Christoph Blume danken, dass er mich nach meinem Interesse gleich in seine Arbeitsgruppe aufgenommen hat, mit seinem Fachwissen jederzeit eine Antwort auf alle Fragen geben konnte und viel Geduld mit dem Fertigstellen meiner Arbeit gezeigt hat. Außerdem bin ich sehr dankbar, dass ich die Erfahrungen machen durfte u.a. eine Woche am ALICE Detektor vorort mitzuwirken und einen Workshop in Turin mitzumachen.

Ein großes Dankeschön von ganzem Herzen gilt Benjamin Dönigus. Er hat mich von Anfang an für dieses interessante Thema begeistert und hat mich als Betreuer der Arbeit ebenfalls mit seiner Expertise stets unterstützt und gefördert. Hier kann ich wirklich glücklich sein so eine super Betreuung zu haben. Was ich zudem sehr zu schätzen weiß ist, dass er auch in schwierigen privaten Themen immer ein offenes Ohr hatte. Danke Dir dafür!

Ömür, Benedikt, Esther, Guido und Pascal möchte ich ebenfalls ein Danke aussprechen, da sie in den TRD und Nuclei Themen neben Benjamin die ersten Ansprechpartner gewesen sind.

Meinen aktuellen und ehemaligen Bürokollegen Behruz, Julian, Heidi und Büronachbarn Flo möchte ich ebenfalls danke sagen, nicht nur für das Weiterhelfen in verschiedensten ROOT- und Physikfragen, sondern auch für viele lustige Momente mit den ein oder anderen Hopfenerzeugnissen, oder auch dem ein oder anderen Mozzarella Stick. Dazu zählen auch die Kollegen der ALICE Gruppe Basti, Stefan, Carsten, Patrick, Adrian, etc. die einerseits mit ihrer Erfahrung in physikalischen Problemen weiterhelfen konnten, aber auch die gemeinsame Zeit auf Meetings, Konferenzen, Ausflügen und Feierabenden zu unvergesslichen Momenten gemacht haben.

Danken möchte ich auch David, Max, Anna und Leslie, die mir in den ersten Semestern immer zur Seite standen. Es freut mich immer zu hören, wie es mittlerweile bei euch läuft in der Beratung, beim Fliegen, der Doktorarbeit und bei den Management Themen der Gastro.

Meiner Familie bin ich für ihren bedingungslosen Rückhalt unendlich dankbar; meiner Mutter, die mir immer die Freiheit der Selbstbestimmung gibt; meiner Schwester, die

immer wieder hinterfragt wie es läuft und mich so in die richtige Bahn bringt. Die größte Motivation für den ganzen Weg bis hierher hat mir wohl mein Vater gegeben, der mit seinem Verständnis von Naturwissenschaften auch immer großes Interesse an meiner Arbeit gezeigt hat. Ich wäre so stolz dir das Endergebnis zeigen zu können. Ich vermisste dich.

Schließlich bin ich auch meinen besten Freunden Luis, Christian und Stefan für so vieles dankbar. Ihr steht mir in allen Zeiten zur Seite, sei es private Themen, sei es Hürden in der Uni oder sei es der Rückhalt im Fußball um diese Arbeit fertigzustellen. Danke Euch, Jungs!

Erklärung

nach §28 (12) Ordnung für den Bachelor- und den Masterstudiengang Physik

Hiermit erkläre ich, dass ich diese Arbeit selbstständig und ohne Benutzung anderer als der angegebenen Quellen und Hilfsmittel verfasst habe. Alle Stellen der Arbeit, die wörtlich oder sinngemäß aus Veröffentlichungen oder aus anderen fremden Texten entnommen wurden, sind von mir als solche kenntlich gemacht worden. Ferner erkläre ich, dass diese Arbeit nicht - auch nicht auszugsweise - für eine andere Prüfung verwendet wurde.

Benjamin Brudnyj, Frankfurt am Main, den 26. Juni 2019

